OPTICS

Optical coherence transfer mediated by free electrons

Ofer Kfir[1,2]*, Valerio Di Giulio[3], F. Javier García de Abajo[3,4], Claus Ropers[1,2]

We theoretically investigate the quantum-coherence properties of the cathodoluminescence (CL) emission produced by a temporally modulated electron beam. Specifically, we consider the quantum-optical correlations of CL produced by electrons that are previously shaped by a laser field. Our main prediction is the presence of phase correlations between the emitted CL field and the electron-modulating laser, even though the emission intensity and spectral profile are independent of the electron state. In addition, the coherence of the CL field extends to harmonics of the laser frequency. Since electron beams can be focused to below 1 Å, their ability to transfer optical coherence could enable the ultra-precise excitation, manipulation, and spectrally resolved probing of nanoscale quantum systems.

INTRODUCTION

Inelastic electron scattering constitutes the basis of various powerful spectroscopy and spectrally selective imaging techniques (*1*). Cathodoluminescence (CL) and electron energy-loss spectroscopy (EELS) are related approaches for harnessing the spectral density of spontaneous interaction processes (*1*, *2*). In CL, the photon emission process involves no external field other than that provided by the electron, so there is no reference to compare the emission phase with. CL emission has spatial and temporal coherences (*3*–*9*) that represent phase correlations in space and time, respectively, with an absolute phase that may differ for each realization. In EELS, the incident and inelastically scattered electron states lose their coherence through the random phase associated with the resonant excitation. A stimulated counterpart for EELS interactions has been established in the form of photon-induced near-field electron microscopy (PINEM) (*10*–*12*) or electron energy-gain spectroscopy (EEGS) (*13*, *14*). In these techniques, the external excitation of a particular mode increases its interaction probability and thus selectively enhances the sensitivity for probing or imaging (*15*, *16*). The coherence of the electron-energy states is evident in a transverse (*17*–*19*) or longitudinal structuring of the electron beam as attosecond pulses (*20*–*23*). Recent work (*24*) has used semi-classical arguments to conclude a dependence of the excitation probability of two-level systems initially in the ground state by an individual electron on its wave function, although such dependence disappears in a full quantum treatment of the system (*25*). For CL, a quantum description of its properties should adhere to our current understanding, in which a point-particle description of the electron is sufficient. By addressing the quantum nature of the electron, one can ask how and to what extent would properties of CL, such as its intensity, coherence characteristics, and radiation pattern (*26*–*28*), be affected by the incident state of the electron.

Here, we directly address these questions in a rigorous theoretical framework, making predictions for the quantum state of radiation produced by phase- and density-modulated electron states. Establishing that an electron beam can coherently stimulate optical excitations, we introduce the notion of "electron-mediated coherence transfer." Specifically, our results show that the temporal shaping of an electron beam has profound and measurable consequences for inelastic electron-light scattering. In the single-electron limit, we demonstrate that the coherence properties and the quantum-optical correlations strongly depend on the details of the electron state, while the CL intensity and spectral profile remain unaffected by the electronic wave function. In particular, we show that CL emission produced by PINEM-modulated electrons can exhibit mutual coherence with a replica of the PINEM-driving optical field or with its harmonics. We propose interferometric measurements for the extraction of phase information in CL by homodyne tomography of the radiation quantum state. The results are readily applicable not only to generated radiation such as CL but also to polarization created in nonradiative states such as deep-subwavelength excitation of higher-order multipoles (*29*). This concept defines a way of transferring optical polarization carried by electrons, which allow for sub-nanometer precision. Our study could also illuminate the role of single electrons in multi-electron bunches, which, according to several recent proposals (*24*, *30*–*34*), may be used for accessing and manipulating individual quantum systems.

RESULTS AND DISCUSSION

Figure 1 represents a conceptual system to investigate coherent CL, which can be implemented within an electron microscope. Optical phase information from a PINEM-driving laser field is imprinted on and carried by the electron over a distance z, resulting in a coherent CL emission by interaction with an out-coupling sample system. Such electron transfer of optical coherence can be detected by an interferometric setting that targets either the linear or the nonlinear response of free electrons (Fig. 1, B and C, respectively).

We first consider comb-like electron-energy superposition states combined with the radiation vacuum $|0\rangle$

$$|\psi_{in}\rangle = |0\rangle \otimes \sum_{j=-\infty}^{\infty} c_j |E_j\rangle = \sum_{j=-\infty}^{\infty} c_j |E_j, 0\rangle \quad (1)$$

where c_j are the complex probability amplitudes for electron states with energy E_j, and the index j runs over electron-energy levels. The coefficients c_j are normalized as $\sum_j |c_j|^2 = 1$, and their phases vary with electron propagation in vacuum according to the free-particle dispersion. The quantum-optical and coherence properties of the CL from an electron state with a temporally modulated density depend on the interaction of the electron with an emitter. For simplicity, we

[1]University of Göttingen, IV. Physical Institute, Göttingen, Germany. [2]Max Planck Institute for Biophysical Chemistry (MPIBPC), Göttingen, Germany. [3]ICFO—Institut de Ciencies Fotoniques, The Barcelona Institute of Science and Technology, 08860 Castelldefels, Barcelona, Spain. [4]ICREA—Institució Catalana de Recerca i Estudis Avançats, Passeig Lluís Companys 23, 08010 Barcelona, Spain.
*Corresponding author. Email: ofer.kfir@mpibpc.mpg.de

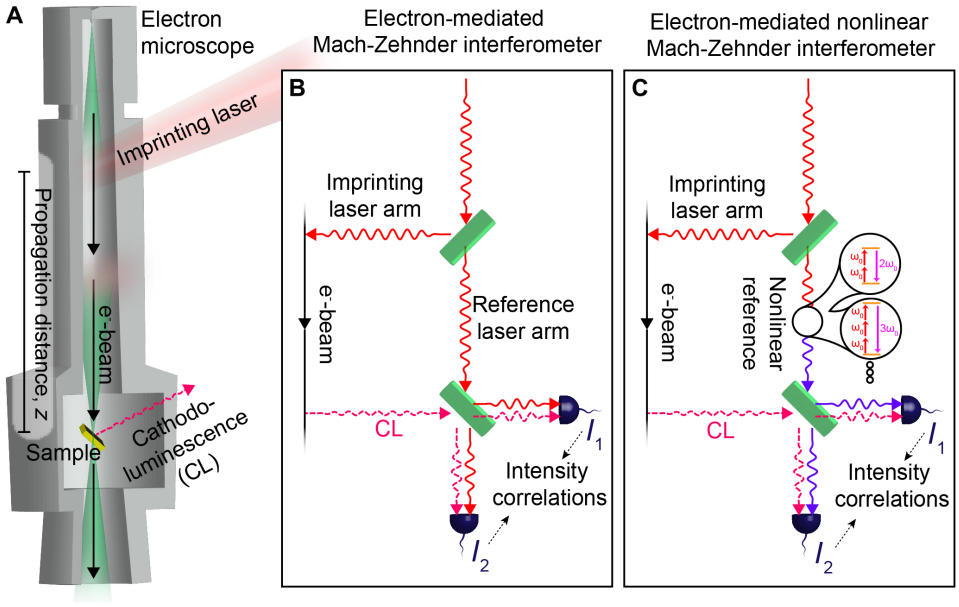

Fig. 1. Linear and nonlinear Mach-Zehnder interferometer incorporating a free-electron beam. (**A**) Proposed experimental concept based on an electron beam (e-beam, illustrated in green) in a transmission electron microscope. A laser field imprints optical-phase information on the electron, which, after propagation, can transfer it back to the radiation via CL emission, typically near the sample section of the microscope. (**B**) Scheme for a Mach-Zehnder interferometer with a reference laser and optical coherence carried by a free-electron beam. Intensity correlations between the two interferometer ports, measured as I_1 and I_2, are used to retrieve information on the electron arm of the interferometer, as well as on the sample. (**C**) Nonlinear Mach-Zehnder interferometry can reveal information on high-order components of the electron state and the CL by interfering with harmonic frequencies of the reference field.

consider a single nondegenerate optical band into which CL is emitted. General expressions for the quantum properties of the CL are derived in Materials and Methods, including the radiation continuum, as well as states with definite momentum, energy, and polarization. The photon frequency represents a good quantum number within the interaction bandwidth because it is a single-valued function of the longitudinal momentum. Transverse deflections can be neglected under the nonrecoil approximation (*34*), which is valid for the examples that we discuss here. The quantum-optical properties of the CL emission can be described by the scattering operator, $\hat{\mathcal{S}}$, which, under the above conditions, has the form of a displacement operator

$$\hat{\mathcal{S}} = \exp\left[\int_0^\infty d\omega\left(g_\omega \hat{b}_\omega \hat{a}_\omega^\dagger - g_\omega^* \hat{b}_\omega^\dagger \hat{a}_\omega\right)\right] \quad (2)$$

as derived for classical and quantum fields (*20*, *36*). For every frequency, the scattering operator allows for annihilation and creation of a photon, marked by the operators $\hat{a}_\omega$ and $\hat{a}_\omega^\dagger$, where energy is conserved by the corresponding electron-energy ladder operators $\hat{b}_\omega^\dagger$ and $\hat{b}_\omega$, respectively. Here, g_ω accounts for the electron-photon coupling at the angular frequency ω, where the photon spectral density of the CL is given by $|g_\omega|^2$. Similarly, $|g_\omega|^2$ would be the EELS spectral density in the absence of competing loss mechanisms (e.g., bulk plasmons and incoherent emissivity). The phase of g_ω is arbitrary, and g_ω can be chosen as a non-negative real-valued spectral function. However, in examples such as the radiation into normal modes of a fiber, it is convenient to impose a flat spectral phase on the photonic modes and place the spectral degree of freedom as a complex coupling function. A rigorous derivation of Eq. 2 and the conditions for which it applies are given in Materials and Methods ("Evolution operator" section).

The final quantum state $|\psi_f\rangle = \hat{\mathcal{S}}|\psi_{in}\rangle$, which can be calculated for an arbitrary coupling strength, is used to obtain the properties of the CL emission (see the "Generalization for strong electron-photon coupling" section). One can gain some intuition from the first-order approximation in the weak electron-photon coupling regime, $|g_\omega|^2 \ll 1$, for which the final state is

$$|\psi_f\rangle \approx \sum_j c_j\left[|E_j, 0\rangle + \int_0^\infty d\omega\, g_\omega |E_j - \hbar\omega, 1_\omega\rangle\right] \quad (3)$$

The weak interaction has a small probability amplitude to create a photon with angular frequency ω, represented by state $|1_\omega\rangle$, accompanied by a corresponding electron-energy loss. Notably, the CL intensity is unaffected by the specific electron superposition state

$$\langle \hat{n}_\omega \rangle = \langle \hat{a}_\omega^\dagger \hat{a}_\omega \rangle = \sum_{j=-\infty}^{\infty} |c_j|^2 |g_\omega|^2 = |g_\omega|^2 \quad (4)$$

(see derivation for continuous spectrum in the "Mean number of excitations after interaction" section). The expectation value for an operator refers to the final electron-photon state, $\langle \hat{O} \rangle \equiv \langle \psi_f | \hat{O} | \psi_f \rangle$. Equation 4 complies with the current understanding of CL and, thus, provides for a solid scientific basis for the predictions in this work. In contrast to the wave function–independent photon emission probabilities, the expectation value for the electric field carries information on the electron temporal structure. The physical electric field at a particular frequency ω and time $t = 0$ is $\vec{\mathbf{E}}_\omega = \langle \hat{\vec{\mathbf{E}}}_\omega \rangle$ and can be represented as a sum of two complex components, $\vec{\mathbf{E}}_\omega = \vec{\mathbf{E}}_\omega^{(+)} + \vec{\mathbf{E}}_\omega^{(-)}$, with $\vec{\mathbf{E}}_\omega^{(-)} = (\vec{\mathbf{E}}_\omega^{(+)})^\dagger$. The field's amplitude is proportional to the expectation value of a ladder operator

$$\langle \hat{E}_\omega^{(+)} \rangle \propto \langle \hat{a}_\omega \rangle \quad (5)$$

The proportionality makes it convenient to represent the field with the ladder operator, $\hat{a}_\omega \equiv \hat{a}_{\omega,(t=0)}$, since $\hat{a}_\omega$ relates directly to the photon statistics (e.g., shot noise in an interferometer). This procedure is justified if the effects of the spatial distribution and the polarization of the field can be traced out, as in CL into single-mode fibers (see the exact expression in the "Mean electric field after interaction" section). Evaluating the photonic ladder operator for $|\psi_f\rangle$ in Eq. 3, we find

$$\langle \hat{a}_\omega \rangle = \sum_{j,j'=-\infty}^{\infty} c_j^* c_{j'} g_\omega \langle E_j, 0 | E_{j'} - \hbar\omega, 0 \rangle \tag{6}$$

We assume that the PINEM-driven state is a comb separated by the photon energy, $\hbar\omega_0$, where the electron spectral density distribution is much narrower than the separation of the levels. Thus, one can use discrete level indices (*37*) and write $\langle E_j | E_{j'} - \hbar\omega \rangle = \delta_{E_j, E_{j'} - \hbar\omega} = \delta_{j', j+n}$, where n is the energy exchange in terms of a harmonic of the fundamental ladder separation, $n = \omega/\omega_0$. Substituting the Kronecker δ into Eq. 6 yields a simple expression for the field

$$\langle \hat{a}_\omega \rangle = \begin{cases} g_{n\omega_0} \sum_{j=-\infty}^{\infty} c_j^* c_{j+n} & \omega = n\omega_0, n \in \mathbb{Z} \\ 0 & \text{otherwise} \end{cases} \tag{7}$$

Since c_j are the amplitudes of the energy states E_j, they are proportional to the Fourier coefficients of the electron wave function, that is, $c_j \equiv \langle E_j | \psi \rangle \propto \int \psi(t) e^{ij\omega_0 t} dt$, which can be used to simplify the CL field

$$\langle \hat{E}_\omega^{(+)} \rangle \propto \langle \hat{a}_\omega \rangle = g_\omega \mathcal{FT}[|\psi(t)|^2]_{(\omega)} \tag{8}$$

Incidentally, the temporal electron-probability amplitude, $\psi(t)$, can be represented spatially along the propagation axis $\overline{\psi}(z) = \psi(t = z/v)$ using the electron group velocity v. Equation 8 is a central result of this paper, representing a general property of CL from a structured electron state (see detailed calculation in the "Mean electric field after interaction" section). We emphasize that only the expectation value of the field follows the electron density, whereas the mean photon number, $\langle \hat{n}_\omega \rangle$, is unaffected by the electron temporal structure (see Eq. 4). In addition, higher-order correlations are more intricate (see derivation in the "Higher-order correlations" section)

$$\langle (\hat{a} - \langle \hat{a} \rangle)^N \rangle = g_\omega^N \sum_k \binom{N}{k} \mathcal{FT}[|\psi(t)|^2]_{(k\omega)} \cdot \left(-\mathcal{FT}[|\psi(t)|^2]_\omega\right)^{N-k} \tag{9}$$

where $\binom{N}{k}$ are Newton's binomial coefficients. To quantify the coherence properties of the emitted CL, we propose the "degree of coherence" (DOC) as a measure of the local optical power density carried by a field with a well-defined phase compared to the energy density at a given frequency. More precisely

$$\begin{aligned} \mathrm{DOC}(\omega) &= \frac{\langle \hat{E}_\omega^{(-)} \rangle \langle \hat{E}_\omega^{(+)} \rangle}{\langle \hat{E}_\omega^{(-)} \hat{E}_\omega^{(+)} \rangle} = \frac{\langle \hat{a}_\omega^\dagger \rangle \langle \hat{a}_\omega \rangle}{\langle \hat{a}_\omega^\dagger \hat{a}_\omega \rangle} \\ &= \left| \mathcal{FT}\left[|\psi(t)|^2 \right]_{(\omega)} \right|^2 \end{aligned} \tag{10}$$

Obviously, for a coherent state of light (*38*), the degree of coherence is unity. Furthermore, the above expression remains unchanged for a continuous electron-energy spectrum as expressed in the "Degree of coherence" section.

Let us further explore the predictions of Eq. 10. First, although the DOC is defined as a local property of the CL emission, it depends purely on the properties of the luminescing electron, and not on the material or the geometry of the electron-light coupler. The local electromagnetic energy density in the denominator of Eq. 10 establishes the DOC as an invariant property of a given electron density $|\psi(t)|^2$, regardless of the spatial profile of the CL emission. Since spatially varying electron profiles still require temporal density modulations to have a nonzero DOC, we refrain from discussing the complexities that spatial and spatio-temporal effects may add. Second, we have $\mathrm{DOC}(\omega = 0) = 1$, since the electron wave function is normalized. Third, the CL field is proportional to $\sqrt{\mathrm{DOC}(\omega)}$ and, thus, to the electron probability density. The coherent fraction of the CL power is proportional to the square of the temporal electron density. Therefore, dense electron distributions are preferred, as in the form of short electron pulses [e.g., full width at half maximum (FWHM) of 200 fs, as experimentally shown in (*39*)]. We note that the coherent CL field emitted from such a pulsed electron must be pulsed as well, with an equal duration; thus, the FWHM of the optical intensity is shorter by a factor of $\sqrt{2}$.

Figure 2 presents a sinusoidal modulation of the electron through PINEM and the resulting properties of the DOC for the emitted radiation. In particular, Fig. 2A illustrates a PINEM-driving laser field that imprints an oscillatory phase (orange) on the electron, without an immediate change in the electron density (gray). The electron-phase curvature represents a varying velocity, Δv, which acts as temporal lensing that modulates the electron probability density after propagation. CL (e.g., into an aligned waveguide) should be locked to the phase of the modulated electron and, therefore, to the phase of the driving field. The electron arrival time does not affect the locking to the phase of the PINEM-driving laser, as illustrated by the few electron replicas sketched in Fig. 2A as ellipsoids. Figure 2B shows the DOC for CL from a PINEM-modulated electron, as a function of the propagation distance, z, to the CL emitter. For this numerical simulation, we used a standard electron beam acceleration voltage of 200 keV, a wavelength of 800 nm ($\hbar\omega_0 = 1.55$ eV), and an easily accessible PINEM parameter $|\beta| = 4$, such that the electron phase modulation at $z = 0$ is given by $e^{-2|\beta| i \cos \omega_0 t}$. In particular, Fig. 2B presents the sum $\sum_j (c_j(z))^* c_{j+n}(z)$, which is nonzero only for harmonics of the modulating laser, as predicted by Eq. 7. Here, the initial amplitudes of the electron state are the Bessel functions of the first kind (*20*, *36*), $c_j(z = 0) = J_j(2|\beta|)$, corresponding to the Fourier transform of the oscillatory electron phase. The coefficients c_j evolve in vacuum as $c_j(z) = c_j(0) e^{ik_z z}$, where $\hbar k_z$ is the electron momentum for energy E_j and $\hbar$ is the reduced Planck constant (see the "Degree of coherence for a PINEM-modulated electron" section for an explicit representation). We note that, in some of the literature, β (occasionally marked g) is referred to as "the coupling coefficient" in PINEM experiments, as it couples adjacent electron-energy levels by stimulated emission and absorption of laser photons. The coupling in this work, g_ω, is the coefficient for exchanging electron-energy loss with spontaneous photon emission, assuming negligible losses. These two quantities are linked, as described previously (*36*, *37*): if one populates our conceptual CL emitter with a coherent state having a mean of $\langle n \rangle$ photons at frequency ω and use it to drive electrons, the effective PINEM parameter would be $\beta = g_\omega \sqrt{\langle n \rangle}$. Figure 2C focuses on a particular propagation distance $z = 6.43$ mm (marked with a white dashed line in Fig. 2B), where the CL spectrum is widest. Aside from the z dependence, the peak value of the DOC is fixed and located at exact integer multiples of ω_0. The distribution in the vicinity of the harmonics is determined by the duration of the pre-structured electron, as plotted in Fig. 2C for Gaussian

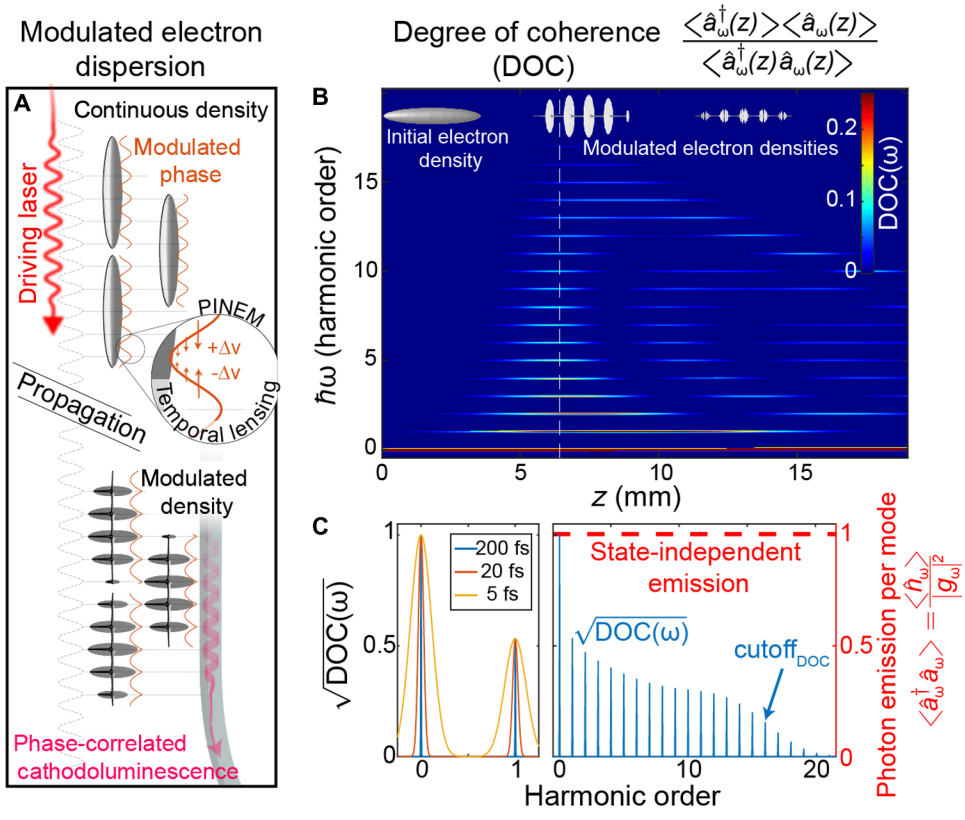

Fig. 2. Coherent properties of CL emission by shaped electrons. (**A**) (Top) Laser-driven PINEM imprints phase oscillations on an electron wave packet, regardless of the exact arrival timing of the electron. The electron-phase oscillations are equivalent to a temporal lens, slowing and accelerating parts of the wave packet periodically. (Bottom) After propagation, anharmonic density and phase modulations evolve in the electron, leading to coherent CL (e.g., in a waveguide). (**B**) Calculated evolution of the degree of coherence (DOC) following PINEM as a function of the propagation distance *z*. The DOC is nonzero only for harmonics of the PINEM-driving laser. The cutoff of the harmonic DOC spectrum is determined by the span of the electron-energy ladder population. For PINEM-modulated electron, the cutoff harmonic order is $\text{cutoff}_{\text{DOC}} \approx 4|\beta| = 16$. (**C**) The emitted field is proportional to $\sqrt{\text{DOC}}$, and its width is inversely proportional to the pulse duration of the pre-structured electron density (see legend for FWHM electron pulse durations). While the DOC and its square root comprise a harmonic frequency comb that varies with *z*, the emission rate of CL photons (red dashed line) remains unaffected by the temporal structure and only depends on the coupling amplitude, g_ω, between the electron and the optical modes. The panels in (C) refer to $z = 6.43$ mm [white dashed line in (B)].

electron pulses. Taking Fig. 2C to two of its extremes, if the electron pulse duration is infinitely long, the DOC is nonzero only at an infinitesimal band for each harmonic. In contrast, if the electron is infinitely compressed to a point-like particle, the DOC of the various harmonics merge, and the CL is fully coherent. For a PINEM-driven modulation, the CL field (proportional to $\sqrt{\text{DOC}}$) can reach nearly 50% coherence for many harmonic orders (blue curve in Fig. 2C). The CL emission rate, normalized to the coupling probability, is independent of frequency (red dashed curve), as expressed in Eq. 4.

To offer a quantitative example, we consider CL into a parallel dielectric waveguide (*36*, *40*) produced by a 200-fs-long Gaussian electron pulse that is modulated by PINEM. Our interest in this particular system is explained at a later stage. The waveguide parameters are chosen such that the phase velocity of the optical mode at the frequency of the PINEM-driving laser equals the electron group velocity. For electrons accelerated to 200 keV(corresponding to 69% of the speed of light in vacuum), we find that for electrons passing near the surface of a cylindrical silicon-nitride waveguide, the coupling is most efficient for a diameter of 345.8 nm. Figure 3 describes such an experiment. The CL field, E_{CL}, can be collected in a waveguide and mixed with a replica of the driving laser (red), E_R, using a 50/50 beam splitter. Figure 3B shows the coupling $|g_\omega|$ alongside the emitted field $|\langle \hat{a}_\omega\rangle|$ for electrons that propagate for 30 μm near the waveguide surface. In such Mach-Zehnder interferometry between weak and strong inputs, the difference collected by two detectors, I_1 and I_2 (see the "On the calculation of quantum averages of time-dependent field operators" section), is proportional to the CL field $(I_2 - I_1) \approx 2\Re e[E_R E_{\text{CL}}]$. The shot noise of the strong reference field dominates each detector. However, the noise is correlated since the reference field photon fluctuations distribute evenly in the beam splitter. Thus, the dominant reference noise vanishes when subtracting the signal of the two detectors (see the "Intensity and noise in a balanced detection experiment for finite electron and laser pulses" section). This homodyne detection scheme uses the reference laser for the analysis of a weak coherent-CL signal with shot-noise sensitivity (*41*). In addition, since the noise of the reference pulse is suppressed, there is no strict requirement that the reference pulse matches the electron pulse duration. The reference simply needs to overlap with the CL pulse. The next nonzero term of the noise (see the "Intensity and noise in a balanced detection

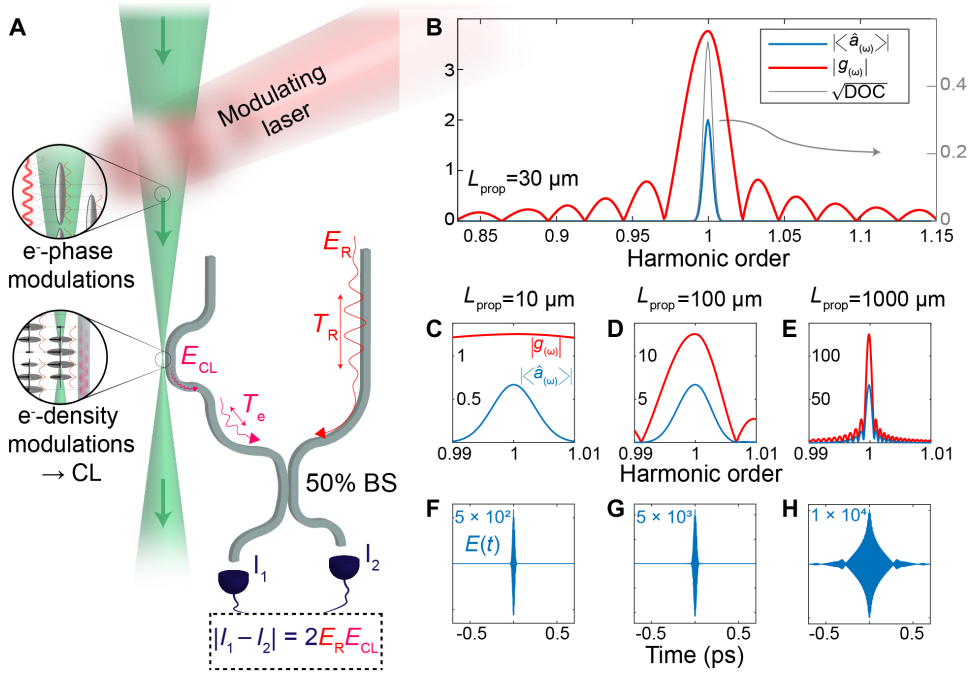

Fig. 3. Correlations in the CL into a dielectric waveguide produced by modulated electrons. (**A**) Conceptual scheme of the experimental setting on the basis of photonic circuitry. A laser field structures a pulsed electron beam, which excites coherent radiation in a parallel-aligned waveguide. Mixing a replica of the driving laser field, E_R, with the CL field, E_{CL}, results in a difference between the signals recorded in the detectors at the output ports of the interferometer, I_1 and I_2. (**B**) Properties of CL emitted into the waveguide for an interaction length of 30 μm positioned at a distance $z = 6.43$ mm away from the electron modulation region. The coherent CL amplitude (blue) is the product of the spectral coupling amplitude, $|g_\omega|$ (red), and $\sqrt{\mathrm{DOC}(\omega)}$ (gray), where phase matching between the electron and the guided modes limits the CL emission to a single harmonic peak. (**C**) to (**H**) show CL properties as a function of the propagation length near the fiber, L_{prop}: (C) to (E) show the spectral distribution of $|g_\omega|$ and $\langle \hat{a}_\omega \rangle$, whereas (F) to (H) show the emitted CL-field pulse in the time domain, $E(t)$. The different columns show the CL properties for an electron propagation length $L_{prop} = 10$ μm (C and F), 100 μm (D and G), and 1 mm (E and H) along the waveguide. The effect of L_{prop} on the peak probability of emission is reflected in the vertical scale. When the coupling bandwidth is narrower than the width of the DOC [e.g., in (E)], the CL pulse is temporally distorted (H). Details of the coupling into a cylindrical waveguide are presented elsewhere (*36*).

experiment for finite electron and laser pulses" section) can be smaller by orders of magnitude. Consequently, the limiting factor in an experiment would be the buildup of noise originating from the imperfect or imbalanced quantum efficiency of the two detectors and from intensity fluctuations of the reference laser field (*42*).

Figure 3 (C to E) depicts the amplitudes of the coupling and the field for various propagation lengths of the electron in the near field of the waveguide, alongside the emitted CL field in Fig. 3 (F to H). We note that for a long propagation path along the fiber, the degree of coherence (blue) can be wider than the CL coupling g_ω (red), leading to a lower signal-to-noise ratio (SNR) and distortions in the temporal shape of the CL field, as shown in Fig. 3H. In such a case, the CL-field emission is optimal for longer electron pulses that match better to the bandwidth of the coupling.

Generally, all of our results are applicable to scenarios with multiple modes, including free-space radiation from surfaces and nanostructures, which are typically characterized by CL. However, choosing CL into a parallel waveguide as the main example in this work has a few instructional, conceptual, and practical merits: (i) An optical fiber can carry a single transverse mode that allows for a straightforward and mode-matched interferometric detection of the field. (ii) The coupling has a simple form, similar to a sinc function. (iii) The coupling can be made strong by macroscopic phase matching between the free electron and the radiation, which could enable the detection of CL from even a single electron. A similar logic was applied to radiation-driven electrons by elongated phase matching near dielectric surfaces (*43*, *44*). (iv) The interaction length provides for a continuous tuning knob to control the coupling bandwidth. (v) Dielectric waveguides can be decoupled from the radiation they host and maintain photon entanglement over many kilometers (*45*). Thus, the CL photons maintain quantum correlations with the electron (*36*), which may be lost if the CL is mediated by lossy polaritonic modes such as plasmons (*6*). (vi) The low dimensionality of a parallel waveguide allowed us to focus this work on temporally modulated electron wave functions. More generally, the consequences of imprinting temporal phases on electrons are extendable to scenarios that spatio-temporally manipulate the electron beam (*17*–*19*). The CL field emitted at optical frequencies from a static transverse structuring of the electron wave functions [e.g., bipolar or vortex beams (*46*, *47*)] has spatial correlations, but the expectation value of its complex amplitude vanishes [see Eq. 8]. (vii) The emission into a dielectric waveguide is instantaneous and allows us to discuss the basic coherence-transfer mechanism. Additional complexity is added if CL is emitted into a cavity with a comparable or longer lifetime than the electron pulse duration as, for instance, a dielectric microresonator. The collected coherent CL from such objects could carry their temporal and phase signatures in addition to that of the electron.

Conclusions

In conclusion, we have shown that even though the emission rate of CL is independent of the temporal structure of the electron, information embedded on a modulated electron wave function can be retrieved by homodyne mixing with a reference field. Thus, the characterization of the CL emission can reach the shot-noise limit. For a particular emitter, a deviation of the degree of coherence from the calculation shown here can quantify the portion of the incoherent CL emission experimentally. Conceptually, the proposed experimental system is a Mach-Zehnder–like interferometer, mixing the reference light from one arm with the CL-mediated optical coherence carried by the electron in the other arm. We exemplify luminescence into a parallel dielectric waveguide, where CL can be sensitive to even a single electron, and additionally exhibit a narrow linewidth. However, equivalent electron-mediated Mach-Zehnder interferences could be observed using collection systems for CL mounted on scanning and transmission ultrafast electron microscopes, with additional fiber-based or free-space optics. The CL reveals the extreme nonlinear nature of coherence transfer by free electrons, which is capable of emitting a broadband spectrum with intricate correlations, including a degree of coherence for harmonics of the driving field. This concept holds potential for sensitive spectroscopy, as well as for the coherent manipulation of heterostructures and individual quantum systems with femtosecond optical resolution at the atomic scale.

MATERIALS AND METHODS

Evolution operator

We consider an electron beam that is well described by a wave packet localized in momentum space around a wave vector $\mathbf{k}_0$ and that the photon energies involved are small compared with the electron relativistic energy $E_0 = c\sqrt{c^2m^2 + \hbar^2k_0^2}$. We further assume that the electron does not cross the material, which allows us to work in a gauge with zero scalar potential. Thus, the Hamiltonian describing the evolution of the system is (*37*)

$$\hat{\mathcal{H}} = \hat{\mathcal{H}}_0 + \hat{\mathcal{H}}_{\text{int}} \tag{11}$$

$$\begin{aligned}\hat{\mathcal{H}}_0 &= \sum_{\mathbf{k}} [E_0 + \hbar\mathbf{v}\cdot(\mathbf{k}-\mathbf{k}_0)]c_{\mathbf{k}}^{\dagger}c_{\mathbf{k}} \\ &\quad + \int_0^{\infty} d\omega \int d^3\mathbf{r}\hbar\omega\hat{\mathbf{f}}^{\dagger}(\mathbf{r},\omega)\cdot\hat{\mathbf{f}}^{\dagger}(\mathbf{r},\omega) \\ \hat{\mathcal{H}}_{\text{int}} &= \frac{-1}{c}\sum_{\alpha}\int d^3\mathbf{r}\,\hat{J}_{\alpha}(\mathbf{r})\,\hat{A}_{\alpha}(\mathbf{r})\end{aligned} \tag{12}$$

The current operator $\hat{J}_{\alpha}(\mathbf{r}) = (-ev_{\alpha}/V)\sum_{\mathbf{k},\mathbf{q}} e^{i\mathbf{q}\cdot\mathbf{r}} c_{\mathbf{k}}^{\dagger}c_{\mathbf{k}+\mathbf{q}}$ is defined using Fermionic ladder operators $c_{\mathbf{k}}$, and the relativistic electron group velocity $\mathbf{v} = \hbar c^2\mathbf{k}_0/E_0$. m and e are the electron's mass and electric charge, and c is the speed of light in vacuum. E_0 is the electron's initial energy and $k_0 = |\mathbf{k}_0|$. Here, $\alpha = x, y, z$ and $\hat{A}_{\alpha}(\mathbf{r})$ and v_{α} are the projections on axis α of the vector-potential operator at $\mathbf{r}$ and the electron velocity, respectively. V is the volume of the quantization box of the electron. $\hat{\mathbf{f}}(\mathbf{r},\omega)$ is the photonic operator for frequency ω at $\mathbf{r}$. Therefore, the scattering operator governing the evolution of the system from time $t = -\infty$ to $t = \infty$ is given by Di Giulio *et al.* (*34*)

$$\hat{\mathcal{S}}(\infty,-\infty) = e^{i\hat{\chi}(\infty,-\infty)}\hat{\mathcal{U}}(\infty,-\infty)$$

where

$$\begin{aligned}\hat{\mathcal{U}}(\infty,-\infty) &= e^{\int_0^{\infty} d\omega g_{\omega}(\hat{b}_{\omega}\hat{a}_{\omega}^{\dagger} - \hat{b}_{\omega}^{\dagger}\hat{a}_{\omega})} \\ \hat{b}_{\omega} &= \sum_{k_z} c_{k_z}^{\dagger}c_{k_z+\omega/v} \\ \hat{a}_{\omega} &= i\frac{2e\omega}{\hbar g_{\omega}}\int_{-\infty}^{\infty} dz\, e^{-i\omega z/v}\int d^3\mathbf{r}'\sqrt{\hbar\text{Im}\{\epsilon(\mathbf{r}',\omega)\}} \\ &\quad \sum_i G_{z,i}(\mathbf{R}_0,z,\mathbf{r}',\omega)\hat{f}_i(\mathbf{r}',\omega)\end{aligned} \tag{13}$$

$G_{j,i}(\mathbf{r}, \mathbf{r}', \omega)$ is the electromagnetic Green tensor at frequency ω, with $i, j = x, y, z$ satisfying the equation

$$\nabla\times\nabla\times G(\mathbf{r},\mathbf{r}',\omega) - \frac{\omega^2}{c^2}\epsilon(\mathbf{r},\omega)\,G(\mathbf{r},\mathbf{r}',\omega) = \frac{-1}{c^2}\delta(\mathbf{r}-\mathbf{r}').$$

where $\delta(\mathbf{r} - \mathbf{r}')$ is Dirac Delta distribution function. For electrons traveling parallel to the z axis, the Green tensor is rewritten as $G_{z,i}(\mathbf{R}_0, z, \mathbf{r}', \omega)$ to split the coordinate $\mathbf{r}$ into its longitudinal component z and the transverse radius-vector $\mathbf{R}_0$. $\text{Im}\{\epsilon(\mathbf{r}', \omega)\}$ is the imaginary part of the local dielectric constant for an optical frequency ω. k_z is the electron wave-vector projection on the propagation axis, $k_z = \mathbf{k}\cdot\hat{\mathbf{z}}$. We have further assumed an incident focused electron with a transverse component of the wave function satisfying $|\psi_i(\mathbf{R})|^2 \approx \delta(\mathbf{R} - \mathbf{R}_0)$, and $g_{\omega} = \sqrt{\Gamma^{\text{EELS}}(\omega)}$ with $\Gamma^{\text{EELS}}(\omega)$ being the real-valued electron energy-loss probability (*35*). The operator $\hat{\chi}(\infty,-\infty)$ does not need to be specified because it only acts on the electron degrees of freedom (*48*) and it is not of interest for this study. In addition, the previous operators satisfy the following commutation relations

$$\begin{aligned}[\hat{a}_{\omega}, \hat{a}_{\omega'}^{\dagger}] &= \delta(\omega-\omega') \\ [\hat{b}_{\omega}, \hat{b}_{\omega'}^{\dagger}] &= 0 \\ [f_i(\mathbf{r},\omega), f_j^{\dagger}(\mathbf{r}',\omega')] &= \delta(\mathbf{r}-\mathbf{r}')\,\delta(\omega-\omega')\,\delta_{i,j}\end{aligned}$$

which are used in the derivation of the following results. The commutator $[\hat{a}_{\omega}, \hat{a}_{\omega'}^{\dagger}]$ is insensitive to the phase of the optical mode, which allows us to define a non-negative g_{ω}. In the Results and Discussion section, there is a preferred selection of the optical-mode phase, and hence, g_{ω} can be complex. In the example of waveguide modes, as in Fig. 3H, the side lobes are a direct result of a sign flip of g_{ω} within the bandwidth of the coherent emission.

Initial joint electron-sample state

If we consider the incoming electron being in a superposition of energy states and the sample starting from the ground state (i.e., zero photons), the electron-sample initial state in the interaction picture can be written as

$$|\psi(-\infty)\rangle = \sum_{k_z}\alpha_{k_z}|k_z, 0\rangle$$

which corresponds to Eq. 1 expressed as a basis of electron energies. α_{kz} is the coefficient for the momentum component k_z in the electron wave function.

Mean number of excitations after interaction

By evolving the initial state to the final state $|\psi(\infty)\rangle = \hat{\mathcal{S}}(\infty,-\infty)|\psi(-\infty)\rangle$, we can calculate the average number of excitations, which is independent of the electron wave function

$$\langle \hat{a}_\omega^\dagger \hat{a}_\omega \rangle = \langle \psi(\infty) | \hat{a}_\omega^\dagger \hat{a}_\omega | \psi(\infty) \rangle = g_\omega^2$$

Mean electric field after interaction

The quantum average (or the expectation value) of the positive-energy electric field operator, defined as (*49*)

$$\hat{E}_i^{(+)}(\mathbf{r},\omega,t=0) = -4\pi i\omega^2 \int d^3\mathbf{r}' \sqrt{\hbar \mathrm{Im}\{\epsilon(\mathbf{r}',\omega)\}} \times \sum_j G_{i,j}(\mathbf{r},\mathbf{r}',\omega)\hat{f}_j(\mathbf{r}',\omega) \quad (14)$$

which gives

$$\langle \hat{E}_i^{(+)}(\mathbf{r},\omega,t=0)\rangle = 8\pi e\omega M_i(\mathbf{r},\omega)\int_{-\infty}^{\infty} dz\, e^{-i\omega z/v} |\psi(z,t=-\infty)|^2 \quad (15)$$
$$M_i(\mathbf{r},\omega) = \int_{-\infty}^{\infty} dz\, e^{i\omega z/v} \mathrm{Im}\{G_{i,z}(\mathbf{r},\mathbf{R}_0,z,\omega)\}$$

We have introduced the incoming electron wave function in the interaction picture $\psi(z,-\infty) = \sum_{k_z} \alpha_{k_z} e^{ik_z z}/\sqrt{L}$ with L denoting the quantization length. Interestingly, this expression can be recast by using the relation

$$\langle \hat{a}_\omega \rangle = g_\omega \int_{-\infty}^{\infty} dz\, e^{-i\omega z/v} |\psi(z,t=-\infty)|^2$$

This result is equivalent to Eq. 8, and thus

$$\langle \hat{E}_i^{(+)}(\mathbf{r},\omega,t=0)\rangle = 8\pi e\omega \langle \hat{a}_\omega\rangle M_i(\mathbf{r},\omega)/g_\omega \quad (16)$$

Degree of coherence

To quantify the coherence transmitted from the modulated electron to the sample excitations, we define the frequency dependent degree of coherence

$$\mathrm{DOC}(\omega) = \frac{\langle \hat{E}_i^{(-)}(\mathbf{r},\omega,t=0)\rangle\langle \hat{E}_i^{(+)}(\mathbf{r},\omega,t=0)\rangle}{\langle \hat{E}_i^{(-)}(\mathbf{r},\omega,t=0)\hat{E}_i^{(+)}(\mathbf{r},\omega,t=0)\rangle}$$

This quantity can be calculated from Eq. 16 together with the expression

$$\langle \hat{E}_i^{(-)}(\mathbf{r},\omega,t=0)\hat{E}_i^{(+)}(\mathbf{r},\omega,t=0)\rangle = 64\pi^2 e^2\omega^2 |M_i(\mathbf{r},\omega)|^2$$

for the denominator. We find

$$\mathrm{DOC}(\omega) = \frac{\langle \hat{a}_\omega^\dagger\rangle\langle \hat{a}_\omega\rangle}{\langle \hat{a}_\omega^\dagger \hat{a}_\omega\rangle} = \left| \int_{-\infty}^{\infty} dz\, e^{-i\omega z/v} |\psi(z,t=-\infty)|^2 \right|^2$$

as in Eq. 10.

Degree of coherence for a PINEM-modulated electron

It is interesting to study the degree of coherence for an electron that is modulated by free propagation after PINEM interaction with a laser field. Here, we assume a PINEM laser frequency ω_0 and a PINEM coupling parameter β (*1*). In particular, beyond the PINEM interaction region, the electron wave function in the Schrödinger picture reduces to

$$\psi^{(S)}(z,t) = \frac{\phi(z-vt)}{\sqrt{L}} e^{-i\varepsilon_0 t} \sum_{\ell=-\infty}^{\infty} J_\ell(2|\beta|)\, e^{-i\ell\omega_0 t + ik_\ell z + i\arg\{-\beta\}}$$

where $\varepsilon_0 = E_0/\hbar$, $k_\ell = \sqrt{E_\ell^2/c^2 - m^2c^2}/\hbar$ with $E_\ell = E_0 + \hbar\omega_0\ell$, and L is the quantization length (*50*). Therefore, the Fourier components of the wave function are given by

$$\alpha_k^{(S)}(t) = \int_{-\infty}^{\infty} dz\, \psi^{(S)}(z,t)\frac{e^{-ikz}}{\sqrt{L}}$$
$$= \frac{e^{-i\varepsilon_0 t}}{L}\sum_\ell J_\ell(2|\beta|)\, e^{i(k_0-k-2\pi\ell^2/z_T)vt} e^{i\ell\arg\{-\beta\}} \int_{-\infty}^{\infty} d\tilde{z}\, e^{i(k_0+\ell\omega_0/v-k)\tilde{z}}\phi(\tilde{z})$$

We have expanded the wave vector up to second order in ℓ and we have used the fact that the spatial region of interaction is smaller than the Talbot distance z_T, namely, $|z-vt| \ll z_T = 4\pi mv^3\gamma^3/\hbar\omega_0^2$. If we consider an electron pulse of infinite duration, we can approximate $\phi(\tilde{z}) \sim 1$, which yields

$$\alpha_k^{(S)}(t) = e^{-i\varepsilon_0 t}\sum_\ell J_\ell(2|\beta|)\, e^{i(k_0-k-2\pi\ell^2/z_T)vt} e^{i\ell\arg\{-\beta\}}\delta_{k_0+\ell\omega_0/v,k}$$

where we have used the relation $\int dz e^{i(k-k')z} = L\delta_{k,k'}$. We can now move to the interaction picture by multiplying $\alpha_k^{(S)}(t)$ by the factor $e^{i[\varepsilon_0 + v(k-k_0)]t}$. Additionally, by going back to real space, we obtain the electron wave function in the interaction picture

$$\psi(z,t=-\infty) = \sum_\ell J_\ell(2|\beta|)\, e^{-2\pi i\ell^2 d/z_T} e^{i\ell\arg\{-\beta\}} \frac{e^{i(k_0+\ell\omega_0/v)z}}{\sqrt{L}}$$

where we have substituted vt by the propagation distance from the PINEM interaction region d. We are now ready to calculate the Fourier transform of the electron density, which reads

$$\int_{-\infty}^{\infty} dz\, e^{-i\omega z/v}|\psi(z,t=-\infty)|^2 = \sum_{\ell,\ell'} J_\ell(2|\beta|)J_{\ell'}(2|\beta|)\, e^{i(\ell-\ell')\arg\{-\beta\}} e^{-2\pi i(\ell^2-\ell'^2)d/z_T}\delta_{\omega_0(\ell-\ell'),\omega} \quad (17)$$

From Eq. 17, we see that the integral vanishes unless $\omega = n\omega_0$, where n is an integer. With this assumption, we obtain

$$\int_{-\infty}^{\infty} dz\, e^{-i\omega z/v}|\psi(z,t=-\infty)|^2 = e^{in\arg\{-\beta\}} e^{2\pi i n^2 d/z_T}\sum_\ell J_\ell(2|\beta|)J_{\ell-n}(2|\beta|)\, e^{-4\pi i\ell n d/z_T} \quad (18)$$

All the quantities proportional to the Fourier transform in Eq. 18 are calculated for a given harmonic order $n = \omega/\omega_0$.

On the calculation of quantum averages of time-dependent field operators

According to Glauber's prescription (*38*), to calculate averages of time-dependent operators to then compute measurable quantities (e.g., light intensities and correlation functions), the operators have to be understood in the Heisenberg picture. For instance, the time-varying light intensity at a given point in space $\mathbf{r}$ for polarization α has to be calculated as

$$I_\alpha(\mathbf{r},t) = \frac{c}{2\pi}\langle \psi_H | E_\alpha^{H,(-)}(\mathbf{r},t)\, E_\alpha^{H,(+)}(\mathbf{r},t) | \psi_H\rangle$$

where the subscript H stands for Heisenberg picture. Now, by using an adiabatic switching of the interaction, which provides the connection between the interaction and Heisenberg pictures $e^{-i\mathcal{H}t} = e^{-i\mathcal{H}_0 t}\hat{\mathcal{S}}(t,-\infty)$, we can rewrite the average in terms of scattering operators

$$I_\alpha(\mathbf{r},t) = \frac{c}{2\pi}\langle \psi(-\infty)|\hat{\mathcal{S}}^\dagger(t,-\infty)\hat{E}_\alpha^{(-)}(\mathbf{r},t)\hat{E}_\alpha^{(+)}(\mathbf{r},t)\hat{\mathcal{S}}(t,-\infty)|\psi(-\infty)\rangle$$

From the previous expression, it is clear that the scattering matrix $\hat{\mathcal{S}}(\infty,-\infty)$ never appears unless we calculate the intensity at $t = \infty$, which is not the quantity in which one is usually interested. However, a simplification that can be used in this study consists of considering the time-dependent field observables at large times, thus neglecting the few-femtosecond transient period in which the electron is still interacting with the sample and producing nonzero quantum averages of the electric field and light intensity. By doing so, we can extend the final time in the scattering operator to infinity, which leads to

$$I_\alpha(\mathbf{r},t) \approx \frac{c}{2\pi}\langle\psi(-\infty)|\hat{\mathcal{S}}^\dagger(\infty,-\infty)\hat{E}_\alpha^{(-)}(\mathbf{r},t)\hat{E}_\alpha^{(+)}(\mathbf{r},t)\hat{\mathcal{S}}(\infty,-\infty)|\psi(-\infty)\rangle = \frac{c}{2\pi}\langle\hat{E}_\alpha^{(-)}(\mathbf{r},t)\hat{E}_\alpha^{(+)}(\mathbf{r},t)\rangle \quad (19)$$

We lastly remark that all the time-dependent quantities in this work imply this assumption.

Intensity and noise in a balanced detection experiment for finite electron and laser pulses

In this section, we compute the signal and noise in a balanced detection experiment. We assume that a replica of the PINEM-driving laser field is the reference field and that the weak CL emanating from the interaction of the PINEM-modulated electrons with a sample placed downstream is the signal. These two fields are mixed in a symmetric beam splitter, as depicted in Fig. 1. The beam splitter is characterized by reflection and transmission coefficients R and T, which we assume to be independent of the optical frequency or polarization. Subsequently, the total signal is collected by two ideal detectors, labeled D1 and D2, respectively. We write the reference electric field operator as

$$\hat{E}_\alpha^{\mathrm{R}}(\mathbf{r},t) = \int_0^\infty \frac{d\omega}{2\pi}\mathcal{E}_\alpha^{\mathrm{R}}(\mathbf{r},\omega)\,\hat{a}_\omega^{\mathrm{R}}e^{-i\omega t} + \mathrm{h.c.}$$

where the electric field operator connected to the CL emission, $\hat{E}_\alpha^{\mathrm{CL}}(\mathbf{r},t)$, is given by the time-dependent analog of Eq. 14. We remark that the reference field operators $\hat{a}_\omega^{\mathrm{R}}$ and $\hat{a}_\omega^{\mathrm{R}\dagger}$ are assumed to also satisfy the commutation relation $[\hat{a}_\omega^{\mathrm{R}},\hat{a}_{\omega'}^{\mathrm{R}\dagger}] = \delta(\omega-\omega')$. The intensity operator at detector D1 is

$$\hat{I}_\alpha^{\mathrm{D1}}(\mathbf{r},t) = \frac{c}{2\pi}(T^*\hat{E}_\alpha^{(-),\mathrm{CL}}(\mathbf{r},t) + R^*\hat{E}_\alpha^{(-),\mathrm{R}}(\mathbf{r},t)) \times (T\hat{E}_\alpha^{(+),\mathrm{CL}}(\mathbf{r},t) + R\hat{E}_\alpha^{(+),\mathrm{R}}(\mathbf{r},t))$$

Intuitively, the operator $\hat{I}_\alpha^{\mathrm{D2}}$ can be obtained from $\hat{I}_\alpha^{\mathrm{D1}}$ by exchanging the T and R coefficients. The fluence (optical energy per unit area) impinging on each detector is

$$\hat{F}_\alpha^{\mathrm{D1/D2}}(\mathbf{r}) = \int_{-\infty}^{\infty} dt\,\hat{I}_\alpha^{\mathrm{D1/D2}}(\mathbf{r},t)$$

The difference between the two detectors, which is our signal, is given by

$$\mathcal{S} = \langle\hat{F}_\alpha^{\mathrm{D1}}(\mathbf{r})\rangle - \langle\hat{F}_\alpha^{\mathrm{D2}}(\mathbf{r})\rangle = \frac{2ec}{\pi}\mathrm{Re}\left\{(R^*T - RT^*)\int_0^\infty d\omega\,\mathcal{E}_\alpha^{\mathrm{R}*}(\mathbf{r},\omega)\,\alpha^{\mathrm{R}*}(\omega)\,M_\alpha(\mathbf{r},\omega) \times \left(\int_{-\infty}^{\infty} dz\,e^{-i\omega z/v}\,|\,\psi(z,t=-\infty)\,|^2\right)\right\} \quad (20)$$

We redefined here the average $\langle\cdot\rangle$ symbol such that it includes a continuous mode coherent state $|\{\alpha^{\mathrm{R}}\}\rangle$, where $\hat{a}_\omega^{\mathrm{R}}|\{\alpha^{\mathrm{R}}\}\rangle = \alpha^{\mathrm{R}}(\omega)|\{\alpha^{\mathrm{R}}\}\rangle$. $\alpha^{\mathrm{R}}(\omega)$ is the frequency profile of the reference light pulse. One can choose, for example, Fresnel coefficients such as $R = 1/\sqrt{2}$ and $T = i/\sqrt{2}$ to retrieve the homodyne detection signal.

The noise of such a measurement can be calculated similarly. The square of the noise is defined by the variance as

$$\mathcal{N}^2 = \langle[\hat{F}_\alpha^{\mathrm{D1}}(\mathbf{r}) - \hat{F}_\alpha^{\mathrm{D2}}(\mathbf{r})]^2\rangle - \langle\hat{F}_\alpha^{\mathrm{D1}}(\mathbf{r}) - \hat{F}_\alpha^{\mathrm{D2}}(\mathbf{r})\rangle^2 \quad (21)$$

Since we consider a strong reference laser field, $\int_{-\infty}^{\infty}|\alpha^{\mathrm{R}}|^2 d\omega \gg 1$, α^{R} dominates Eq. 21. For the choice $|R| = |T|$, the terms for the noise variance scaling as $|\alpha^{\mathrm{R}}|^4$ and $|\alpha^{\mathrm{R}}|^3$ vanish. Thus, the next leading order is substantially smaller and comprises combinations in which $\hat{E}_\alpha^{\mathrm{R}}$ and $\hat{E}^{\mathrm{CL}}$ appear twice each

$$\begin{aligned}\mathcal{N}^2 = {} & 2\left(\frac{c}{4\pi^2}\right)^2(R^*T - RT^*)^2\int_0^\infty d\omega\int_0^\infty d\omega' \\ & \times \mathrm{Re}\Big\{\mathcal{E}_\alpha^{\mathrm{R}}(\mathbf{r},\omega)\,\alpha^{\mathrm{R}}(\omega)\,\mathcal{E}_\alpha^{\mathrm{R}}(\mathbf{r},\omega')\,\alpha^{\mathrm{R}}(\omega')\Big[\langle\hat{E}_\alpha^{(-),\mathrm{CL}}(\mathbf{r},\omega)\,\hat{E}_\alpha^{(-),\mathrm{CL}}(\mathbf{r},\omega')\rangle \\ & - \langle\hat{E}_\alpha^{(-),\mathrm{CL}}(\mathbf{r},\omega)\rangle\langle\hat{E}_\alpha^{(-),\mathrm{CL}}(\mathbf{r},\omega')\rangle\Big] \\ & + \mathcal{E}_\alpha^{\mathrm{R}}(\mathbf{r},\omega)\,\alpha^{\mathrm{R}}(\omega)\,\mathcal{E}_\alpha^{\mathrm{R}*}(\mathbf{r},\omega')\,\alpha^{\mathrm{R}*}(\omega')\langle\hat{E}_\alpha^{(-),\mathrm{CL}}(\mathbf{r},\omega)\rangle\langle\hat{E}_\alpha^{(+),\mathrm{CL}}(\mathbf{r},\omega')\rangle \\ & - \frac{1}{2}\mathcal{E}_\alpha^{\mathrm{R}}(\mathbf{r},\omega)\,\mathcal{E}_\alpha^{\mathrm{R}*}(\mathbf{r},\omega')\Big[\delta(\omega-\omega') + \alpha^{\mathrm{R}}(\omega)\,\alpha^{\mathrm{R}*}(\omega')\Big]\langle\hat{E}_\alpha^{(-),\mathrm{CL}}(\mathbf{r},\omega)\,\hat{E}_\alpha^{(+),\mathrm{CL}}(\mathbf{r},\omega')\rangle \\ & - \frac{1}{2}\alpha^{\mathrm{R}*}(\omega)\,\alpha^{\mathrm{R}}(\omega')\,\mathcal{E}_\alpha^{\mathrm{R}*}(\mathbf{r},\omega)\,\mathcal{E}_\alpha^{\mathrm{R}}(\mathbf{r},\omega')\langle\hat{E}_\alpha^{(+),\mathrm{CL}}(\mathbf{r},\omega)\,\hat{E}_\alpha^{(-),\mathrm{CL}}(\mathbf{r},\omega')\rangle\Big\}\end{aligned}$$

where $t = 0$ is implicitly understood in the CL operators. The contribution of this leading term to the noise is smaller by the ratio of the reference and CL fields, which could be many orders of magnitude smaller than the shot noise of the reference on each detector. Thus, this result implies a theoretical limit to the noise floor, independent of the intrinsic noise of the detectors. We conclude that the corresponding ideal SNR in this system is SNR = $\mathcal{S}/\mathcal{N}$.

Explicit derivation of Eq. 8

One can separate the initial electron-photon state in Eq. 1 as the product of the electron part $|\psi_e\rangle$ and the vacuum of the radiation, $|\psi_{in}\rangle = |\psi_e\rangle \otimes |0\rangle$, where $|\psi_e\rangle = \sum_j c_j|E_j\rangle$. The ladder coefficients can be derived through simple algebra

$$\langle E_\ell|\psi_e\rangle = \left(\sum_j c_j\underbrace{\langle E_\ell|E_j\rangle}_{\delta_{\ell,j}}\right)$$
$$c_j = \langle E_j|\psi_e\rangle$$

We can now write the sum in Eq. 7 as

$$\begin{aligned}\sum_j c_j^* c_{j+n} &= \sum_j\langle\psi_e|E_j\rangle\langle E_{j+n}|\psi_e\rangle \\ &= \langle\psi_e|\sum_j|E_j\rangle\langle E_{j+n}|\,|\psi_e\rangle \\ &= \langle\psi_e|e^{in\omega_0 t}\sum_j|E_j\rangle\langle E_j|\,|\psi_e\rangle \\ &= \langle\psi_e|e^{in\omega_0 t}|\psi_e\rangle\end{aligned}$$

Here, we assume that the energy states are identical, aside from their energy difference, and that $|\psi_e\rangle$ is fully spanned by the discrete and complete set of $|E_j\rangle$ states, that is

$$|E_{j+n}\rangle = e^{-in\omega_0 t}|E_j\rangle$$
$$\sum_j|E_j\rangle\langle E_j| = \mathcal{I}$$

In the sample region, we can approximate the electron dispersion as linear, and thus, the wave function can be written as a function of time, $\psi(t)$, relying on the relation $z - vt = constant$. Using this temporal electron wave function $\psi(t)$, one finds

$$\begin{aligned}\sum_j c_j^* c_{j+n} &= \int \left(\psi(t)\right)^* e^{in\omega_0 t}\psi(t)dt \\ &= \int |\psi(t)|^2 e^{in\omega_0 t}dt = \mathcal{FT}\left[|\psi(t)|^2\right]_{(n\omega_0)}\end{aligned} \tag{22}$$

Generalization for strong electron-photon coupling

Starting from the scattering operator in Eq. 2, we are interested in the expectation value for a specific frequency Ω, that is, $\langle \hat{a}_\Omega \rangle$, as well as higher-order terms. For this purpose, it is convenient to use the commutation relation

$$[\hat{a}_\Omega, \hat{\mathcal{S}}] = [\hat{a}_\Omega, e^{\int_0^\infty d\omega (g_\omega \hat{b}_\omega \hat{a}_\omega^\dagger - g_\omega^* \hat{b}_\omega^\dagger \hat{a}_\omega)}]$$

Since $\left[\hat{b}_\omega, \hat{b}_{\omega'}^\dagger\right] = \left[\hat{b}_\omega, \hat{\mathcal{S}}\right] = 0$ and

$$\begin{aligned}\left[\hat{a}_\Omega, (g_\omega \hat{b}_\omega \hat{a}_\omega^\dagger - g_\omega^* \hat{b}_\omega^\dagger \hat{a}_\omega)\right] &= \left[\hat{a}_\Omega, g_\omega \hat{b}_\omega \hat{a}_\omega^\dagger\right] \\ &= g_\omega \hat{b}_\omega \delta(\omega - \Omega)\end{aligned}$$

one can use the conditional identity

$$[A, B] = c \Rightarrow [A, e^B] = c\, e^B$$

and write

$$[\hat{a}_\Omega, \hat{\mathcal{S}}] = g_\Omega \hat{b}_\Omega \hat{\mathcal{S}} \tag{23}$$

The expectation value for $\langle \hat{a}_\Omega \rangle$ on the final state, $|\psi_f\rangle = \hat{\mathcal{S}}|\psi_{initial}\rangle = \hat{\mathcal{S}}\sum_j c_j |E_j, 0\rangle$, is

$$\langle \hat{a}_\Omega \rangle = \sum_{j,j'} c_j^* c_{j'} \langle E_j, 0 | \hat{\mathcal{S}}^\dagger \hat{a}_\Omega \hat{\mathcal{S}} | E_{j'}, 0\rangle$$

The commutation relation above allows us to write $\hat{\mathcal{S}}^\dagger \hat{a}_\Omega \hat{\mathcal{S}} = g_\Omega \hat{b}_\Omega + \hat{a}_\Omega$, so

$$\begin{aligned}\langle \hat{a}_\Omega \rangle &= \sum_{j,j'} c_j^* c_{j'} \langle E_j, 0 | g_\Omega \hat{b}_\Omega + \hat{a}_\Omega | E_{j'}, 0\rangle \\ &= g_\Omega \sum_{j,j'} c_j^* c_{j'} \underbrace{\langle E_j, 0 | E_{j'} - \hbar\Omega, 0\rangle}_{\delta_{j,j'-n}, \text{for } n = \Omega/\omega_0} \\ &= g_\Omega \sum_j c_j^* c_{j+n} \\ &\overset{\text{(Eq. 22)}}{=} g_\Omega \mathcal{FT}\left[|\psi(t)|^2\right]_{(\Omega = n\omega_0)}\end{aligned}$$

as in Eq. 8 for weak coupling. We have simplified this expression mostly by using $\hat{a}_\Omega |E_{j'}, 0\rangle = 0$.

Higher-order correlations

The moment of order N for the quantum correlations of the CL is

$$\begin{aligned}\langle (\Delta \hat{a}_\Omega)^N \rangle &= \langle (\hat{a}_\Omega - \langle \hat{a}_\Omega \rangle)^N \rangle \\ &= \sum_k \left\langle \binom{N}{k} \hat{a}_\Omega^k \langle -\hat{a}_\Omega \rangle^{N-k} \right\rangle \\ &= \sum_k \binom{N}{k} (-1)^{N-k} \langle \hat{a}_\Omega \rangle^{N-k} \langle \hat{a}_\Omega^k \rangle\end{aligned} \tag{24}$$

where $\binom{N}{k}$ denotes Newton's binomial coefficients. The operator $\langle \hat{a}_\Omega^k \rangle$ can be simplified using the unitarity of $\hat{\mathcal{S}}$, that is, $\hat{\mathcal{S}}^\dagger \hat{\mathcal{S}} = \hat{I}$, and substituting $\hat{\mathcal{S}}^\dagger \hat{a}_\Omega^k \hat{\mathcal{S}} = (\hat{\mathcal{S}}^\dagger \hat{a}_\Omega \hat{\mathcal{S}})^k$. We find

$$\begin{aligned}\langle \hat{a}_\Omega^k \rangle &= \sum_{j,j'} c_j^* c_{j'} \langle E_j, 0 | \hat{\mathcal{S}}^\dagger \hat{a}_\Omega^k \hat{\mathcal{S}} | E_{j'}, 0\rangle \\ &= \sum_{j,j'} c_j^* c_{j'} \langle E_j, 0 | (\hat{\mathcal{S}}^\dagger \hat{a}_\Omega \hat{\mathcal{S}})^k | E_{j'}, 0\rangle \\ (*) &= \sum_{j,j'} c_j^* c_{j'} \langle E_j, 0 | (g_\Omega \hat{b}_\Omega + \hat{a}_\Omega)^k | E_{j'}, 0\rangle \\ &= g_\Omega^k \sum_{j,j'} c_j^* c_{j'} \underbrace{\langle E_j, 0 | \hat{b}_\Omega^k | E_{j'}, 0\rangle}_{\delta_{j',j+k\Omega/\omega_0}} \\ &= g_\Omega^k \sum_j c_j^* c_{j+k\frac{\Omega}{\omega_0}}\end{aligned}$$

The equation marked with (*) uses the commutation in Eq. 23. We can now substitute $\langle \hat{a}_\Omega^k \rangle$ and $\langle \hat{a}_\Omega \rangle$ in Eq. 24 to write

$$\begin{aligned}\langle (\Delta \hat{a}_\Omega)^N \rangle &= \sum_k \binom{N}{k} (-1)^{N-k} \langle \hat{a}_\Omega \rangle^{N-k} \langle \hat{a}_\Omega^k \rangle \\ &= \sum_k \binom{N}{k} (-1)^{N-k} \left(g_\Omega \sum_j c_j^* c_{j+\frac{\Omega}{\omega_0}}\right)^{N-k} \left(g_\Omega^k \sum_j c_j^* c_{j+k\frac{\Omega}{\omega_0}}\right) \\ &= g_\Omega^N \sum_k \binom{N}{k} (-1)^{N-k} \left(\mathcal{FT}[|\psi(t)|^2]_{(\Omega)}\right)^{N-k} \left(\mathcal{FT}[|\psi(t)|^2]_{(k\Omega)}\right)\end{aligned}$$

REFERENCES AND NOTES

1. A. Polman, M. Kociak, F. J. García de Abajo, Electron-beam spectroscopy for nanophotonics. *Nat. Mater.* **18**, 1158–1171 (2019).
2. L. Reimer, H. Kohl, *Transmission Electron Microscopy: Physics of Image Formation* (Springer Series in Optical Sciences, Springer-Verlag, ed. 5, 2008).
3. S. Meuret, L. H. G. Tizei, T. Cazimajou, R. Bourrellier, H. C. Chang, F. Treussart, M. Kociak, Photon bunching in cathodoluminescence. *Phys. Rev. Lett.* **114**, 197401 (2015).
4. M. Solà-Garcia, S. Meuret, T. Coenen, A. Polman, Electron-induced state conversion in diamond NV centers measured with pump–probe cathodoluminescence spectroscopy. *ACS Photonics* **7**, 232–240 (2020).
5. S. J. Smith, E. M. Purcell, Visible light from localized surface charges moving across a grating. *Phys. Rev.* **92**, 1069 (1953).
6. R. Remez, A. Karnieli, S. Trajtenberg-Mills, N. Shapira, I. Kaminer, Y. Lereah, A. Arie, Observing the quantum wave nature of free electrons through spontaneous emission. *Phys. Rev. Lett.* **123**, 060401 (2019).
7. G. Li, B. P. Clarke, J.-K. So, K. F. MacDonald, N. I. Zheludev, Holographic free-electron light source. *Nat. Commun.* **7**, 13705 (2016).
8. J. Christopher, M. Taleb, A. Maity, M. Hentschel, H. Giessen, N. Talebi, Electron-driven photon sources for correlative electron-photon spectroscopy with electron microscopes. *Nanophotonics* **9**, 4381–4406 (2020).
9. N. J. Schilder, H. Agrawal, E. C. Garnett, A. Polman, Phase-resolved surface plasmon scattering probed by cathodoluminescence holography. *ACS Photonics* **7**, 1476–1482 (2020).
10. B. Barwick, D. J. Flannigan, A. H. Zewail, Photon-induced near-field electron microscopy. *Nature* **462**, 902–906 (2009).
11. S. T. Park, M. Lin, A. H. Zewail, Photon-induced near-field electron microscopy (PINEM): Theoretical and experimental. *New J. Phys.* **12**, 123028 (2010).
12. F. J. García de Abajo, A. Asenjo-Garcia, M. Kociak, Multiphoton absorption and emission by interaction of swift electrons with evanescent light fields. *Nano Lett.* **10**, 1859–1863 (2010).
13. A. Howie, Section 7: Advanced scanning probe techniques-electrons and photons: Exploiting the connection. *Inst. Phys. Conf. Ser.* **161**, 311 (1999).
14. F. J. García de Abajo, M. Kociak, Electron energy-gain spectroscopy. *New J. Phys.* **10**, 073035 (2008).
15. L. Piazza, T. T. A. Lummen, E. Quiñonez, Y. Murooka, B. W. Reed, B. Barwick, F. Carbone, Simultaneous observation of the quantization and the interference pattern of a plasmonic near-field. *Nat. Commun.* **6**, 6407 (2015).
16. P. Das, J. D. Blazit, M. Tencé, L. F. Zagonel, Y. Auad, Y. H. Lee, X. Y. Ling, A. Losquin, C. Colliex, O. Stéphan, F. J. García de Abajo, M. Kociak, Stimulated electron energy loss

and gain in an electron microscope without a pulsed electron gun. *Ultramicroscopy* **203**, 44–51 (2019).
17. G. M. Vanacore, I. Madan, G. Berruto, K. Wang, E. Pomarico, R. J. Lamb, D. McGrouther, I. Kaminer, B. Barwick, F. J. García de Abajo, F. Carbone, Attosecond coherent control of free-electron wave functions using semi-infinite light fields. *Nat. Commun.* **9**, 2694 (2018).
18. G. M. Vanacore, G. Berruto, I. Madan, E. Pomarico, P. Biagioni, R. J. Lamb, D. McGrouther, O. Reinhardt, I. Kaminer, B. Barwick, H. Larocque, V. Grillo, E. Karimi, F. J. García de Abajo, F. Carbone, Ultrafast generation and control of an electron vortex beam via chiral plasmonic near fields. *Nat. Mater.* **18**, 573–579 (2019).
19. A. Feist, S. V. Yalunin, S. Schäfer, C. Ropers, High-purity free-electron momentum states prepared by three-dimensional optical phase modulation. *Phys. Rev. Res.* **2**, 043227 (2020).
20. A. Feist, K. E. Echternkamp, J. Schauss, S. V. Yalunin, S. Schäfer, C. Ropers, Quantum coherent optical phase modulation in an ultrafast transmission electron microscope. *Nature* **521**, 200–203 (2015).
21. K. E. Priebe, C. Rathje, S. V. Yalunin, T. Hohage, A. Feist, S. Schäfer, C. Ropers, Attosecond electron pulse trains and quantum state reconstruction in ultrafast transmission electron microscopy. *Nat. Photonics* **11**, 793–797 (2017).
22. Y. Morimoto, P. Baum, Diffraction and microscopy with attosecond electron pulse trains. *Nat. Phys.* **14**, 252–256 (2018).
23. M. Kozák, N. Schönenberger, P. Hommelhoff, Ponderomotive generation and detection of attosecond free-electron pulse trains. *Phys. Rev. Lett.* **120**, 103203 (2018).
24. A. Gover, A. Yariv, Free-electron–bound-electron resonant interaction. *Phys. Rev. Lett.* **124**, 064801 (2020).
25. Z. Zhao, X.-Q. Sun, S. Fan, Quantum entanglement and modulation enhancement of free-electron-bound-electron interaction. arXiv:2010.11396 (2020).
26. N. Yamamoto, S. Ohtani, F. J. Garcia de Abajo, Gap and Mie plasmons in individual silver nanospheres near a silver surface. *Nano Lett.* **11**, 91–95 (2011).
27. T. Coenen, E. J. R. Vesseur, A. Polman, Angle-resolved cathodoluminescence spectroscopy. *Appl. Phys. Lett.* **99**, 143103 (2011).
28. C. I. Osorio, T. Coenen, B. J. M. Brenny, A. Polmsan, A. F. Koenderink, Angle-resolved cathodoluminescence imaging polarimetry. *ACS Photonics* **3**, 147–154 (2016).
29. M.-W. Chu, V. Myroshnychenko, C. H. Chen, J.-P. Deng, C.-Y. Mou, F. J. García de Abajo, Probing bright and dark surface-plasmon modes in individual and coupled noble metal nanoparticles using an electron beam. *Nano Lett.* **9**, 399–404 (2009).
30. O. Schwartz, J. J. Axelrod, S. L. Campbell, C. Turnbaugh, R. M. Glaeser, H. Müller, Laser phase plate for transmission electron microscopy. *Nat. Methods* **16**, 1016–1020 (2019).
31. I. Madan, G. M. Vanacore, S. Gargiulo, T. LaGrange, F. Carbone, The quantum future of microscopy: Wave function engineering of electrons, ions, and nuclei. *Appl. Phys. Lett.* **116**, 230502 (2020).
32. A. Karnieli, N. Rivera, A. Arie, I. Kaminer, The coherence of light is fundamentally tied to the quantum coherence of the emitting particle. *Sci. Adv.* **7**, eabf8096 (2021).
33. F. J. García de Abajo, V. Di Giulio, Optical excitations with electron beams: Challenges and opportunities. *ACS Photonics* (2021); https://doi.org/10.1021/acsphotonics.0c01950.
34. V. Di Giulio, O. Kfir, C. Ropers, F. J. García de Abajo, Modulation of cathodoluminescence emission by interference with external light. *ACS Nano* (2021); https://dx.doi.org/10.1021/acsnano.1c00549.
35. F. J. García de Abajo, Optical excitations in electron microscopy. *Rev. Mod. Phys.* **82**, 209–275 (2010).
36. O. Kfir, Entanglements of electrons and cavity photons in the strong-coupling regime. *Phys. Rev. Lett.* **123**, 103602 (2019).
37. V. Di Giulio, M. Kociak, F. J. García de Abajo, Probing quantum optical excitations with fast electrons. *Optica* **6**, 1524–1534 (2019).
38. R. J. Glauber, Coherent and incoherent states of the radiation field. *Phys. Rev.* **131**, 2766–2788 (1963).
39. A. Feist, N. Bach, N. Rubiano da Silva, T. Danz, M. Möller, K. E. Priebe, T. Domröse, J. G. Gatzmann, S. Rost, J. Schauss, S. Strauch, R. Bormann, M. Sivis, S. Schäfer, C. Ropers, Ultrafast transmission electron microscopy using a laser-driven field emitter: Femtosecond resolution with a high coherence electron beam. *Ultramicroscopy* **176**, 63–73 (2017).
40. X. Bendaña, A. Polman, F. J. García de Abajo, Single-photon generation by electron beams. *Nano Lett.* **11**, 5099–5103 (2011).
41. H. P. Yuen, V. W. S. Chan, Noise in homodyne and heterodyne detection. *Opt. Lett.* **8**, 177–179 (1983).
42. G. L. Abbas, V. W. S. Chan, T. K. Yee, Local-oscillator excess-noise suppression for homodyne and heterodyne detection. *Opt. Lett.* **8**, 419–421 (1983).
43. R. Dahan, S. Nehemia, M. Shentcis, O. Reinhardt, Y. Adiv, X. Shi, O. Be'er, M. H. Lynch, Y. Kurman, K. Wang, I. Kaminer, Resonant phase-matching between a light wave and a free-electron wavefunction. *Nat. Phys.* **16**, 1123–1131 (2020).
44. M. Kozák, P. Beck, H. Deng, J. McNeur, N. Schönenberger, C. Gaida, F. Stutzki, M. Gebhardt, J. Limpert, A. Ruehl, I. Hartl, O. Solgaard, J. S. Harris, R. L. Byer, P. Hommelhoff, Acceleration of sub-relativistic electrons with an evanescent optical wave at a planar interface. *Opt. Express* **25**, 19195–19204 (2017).
45. S. Wengerowsky, S. K. Joshi, F. Steinlechner, J. R. Zichi, S. M. Dobrovolskiy, R. van der Molen, J. W. N. Los, V. Zwiller, M. A. M. Versteegh, A. Mura, D. Calonico, M. Inguscio, H. Hübel, L. Bo, T. Scheidl, A. Zeilinger, A. Xuereb, R. Ursin, Entanglement distribution over a 96-km-long submarine optical fiber. *Proc. Natl. Acad. Sci. U.S.A.* **116**, 6684–6688 (2019).
46. G. Guzzinati, A. Béché, H. Lourenço-Martins, J. Martin, M. Kociak, J. Verbeeck, Probing the symmetry of the potential of localized surface plasmon resonances with phase-shaped electron beams. *Nat. Commun.* **8**, 14999 (2017).
47. B. J. McMorran, A. Agrawal, I. M. Anderson, A. A. Herzing, H. J. Lezec, J. J. McClelland, J. Unguris, Electron vortex beams with high quanta of orbital angular momentum. *Science* **331**, 192–195 (2011).
48. F. J. García de Abajo, V. Di Giulio, Electron diffraction by vacuum fluctuations. *New J. Phys.* **22**, 103057 (2020).
49. H. T. Dung, L. Knöll, D.-G. Welsch, Three-dimensional quantization of the electromagnetic field in dispersive and absorbing inhomogeneous dielectrics. *Phys. Rev. A* **57**, 3931–3942 (1998).
50. V. Di Giulio, F. J. García de Abajo, Free-electron shaping using quantum light. *Optica* **7**, 1820–1830 (2020).

Acknowledgments
Funding: This work was funded in part by the Deutsche Forschungsgemeinschaft (DFG) in the Collaborative Research Center "Atomic Scale Control of Energy Conversion" (DFG-SFB 1073, project A05) and in the Priority Program "Quantum Dynamics in Tailored Intense Fields" (DFG-SPP 1840), ERC (Advanced Grant 789104-eNANO), the Spanish MINECO (MAT2017-88492-R and SEV2015-0522), the European Commission (project no. 101017720-EBEAM), and the Humboldt Foundation. O.K. acknowledges the Max Planck Society for funding from the Manfred Eigen Fellowship for postdoctoral fellows from abroad. V.D.G. acknowledges support from the EU (Marie Skłdowska-Curie Grant 713729). **Author contributions:** O.K., V.D.G., F.J.G.d.A., and C.R. conceived the concept. O.K. constructed the paper and prepared the figures. O.K. and V.D.G. wrote the paper with contributions from F.J.G.d.A. and C.R. **Competing interests:** The authors declare that they have no competing interests. **Data and materials availability:** All data needed to evaluate the conclusions in the paper are present in the paper and/or the Supplementary Materials. Additional data related to this paper may be requested from the authors.

Submitted 10 November 2020
Accepted 16 February 2021
Published 30 April 2021
10.1126/sciadv.abf6380

Citation: O. Kfir, V. Di Giulio, F. J. Garcia de Abajo, C. Ropers, Optical coherence transfer mediated by free electrons. *Sci. Adv.* **7**, eabf6380 (2021).